



# Combustion characteristics and thermokinetics of coconut shell, coal water slurry, and biomass

Yikun Peng<sup>1</sup> · Xianyou Tang<sup>2</sup> · Zhukai Zeng<sup>1</sup> · Canjun Xu<sup>1</sup> · Wangsong Wu<sup>1</sup>

Received: 31 March 2024 / Accepted: 21 April 2024 / Published online: 1 May 2024  
© Akadémiai Kiadó, Budapest, Hungary 2024

## Abstract

The combustion characteristics of coconut shell, coal water slurry, and biomass were studied by combustion thermogravimetry at different heating rates. The DTG curves of all samples exhibit three distinct peaks. The comprehensive combustion characteristic index ( $S_N$ ) of coconut shell and biomass was higher, and the ignition point and burnout temperature were lower. At the same heating rate, the  $S_N$  of coal water slurry is the highest, the  $S_N$  of coconut shell, coal water slurry and biomass increased by 337%, 259%, and 429%. Based on the distributed Coats–Redfern integral method, the combustion kinetics of the samples was analyzed. The activation energy of low temperature combustion zone is higher than that in high temperature combustion zone. As the heating rate increases, the activation energy of the samples decreases slightly, but the overall trend remains similar. When  $n = 2$ , the fitting curve has a good linear relationship, and the correlation coefficient  $R^2$  is all above 0.99.

**Keywords** Biomass · Coal water slurry · TDA · Kinetic analysis

## Introduction

Coal water slurry is a newer efficient and clean coal-based fuel. It is a mixture of 65% to 70% coal with different particle size distribution, 29% to 34% water and about 1% chemical additives [1, 2]. Through several rigorous processes, sieving impurities such as components that cannot be burned in coal can only retain carbon essence and become the essence of coal water slurry. It has the same fluidity as oil, and its calorific value is half of that of oil, so it is called liquid coal product. The technology of coal water slurry, including the preparation, storage and transportation, combustion, additives, and other key technologies, is a systematic technology

---

✉ Wangsong Wu  
1794123689@qq.com

<sup>1</sup> Zhongnan Engineering Corporation Limited, Power China, Changsha 410021, China

<sup>2</sup> New Energy Holdings Corporation Limited, China General Nuclear, Beijing 100071, China

involving multiple disciplines [3]. Coal water slurry has the characteristics of high combustion efficiency and low pollutant emission. It can be used to replace oil, gas and coal combustion in power station boilers, industrial boilers, and industrial kilns, as well as heating and domestic hot water in hotels, residences, hotels, and office buildings, which is an important part of clean coal technology [4].

Biomass briquetting fuel uses agricultural and forestry wastes as raw materials, through crushing, mixing, extrusion, drying and other processes, to produce a variety of molding (such as block, granular, etc.) can be directly burned a new clean fuel [5]. Biomass briquette fuel is mainly the block fuel produced by processing stem crops, peanut shells, bark, sawdust, and solid wastes (furfural residue, edible fungus residue, etc.). The diameter of biomass pellet fuel is generally 6 to 10 mm, the length is 4 to 5 times of its diameter, the crushing rate is less than 1.5% to 2.0%, the dry basis moisture content is less than 10% to 15%, the ash content is less than 1.5%, the sulfur content and chlorine content are both less than 0.07%, and the nitrogen content is less than 0.5% [6]. The essence of biomass pellet fuel is the direct combustion application of biomass energy, which is the processing and utilization of biomass. Direct combustion can be divided into four types: stove combustion, boiler combustion, garbage combustion and solid fuel combustion [7]. Among them, solid fuel combustion is a new technology, which solidifies biomass and then uses traditional coal-fired equipment. Its advantages are to make full use of biomass energy to replace coal, reduce CO<sub>2</sub> and SO<sub>2</sub> emissions, which is conducive to environmental protection and control of greenhouse gas emissions, slow down the deterioration of the climate and reduce the occurrence of natural disasters [8].

Thermal analysis is a technology based on the measurement and control of thermal properties and temperature of materials [9]. The definition given by the international society for thermal analysis (ICTA) is: thermal analysis is a kind of technology to measure the relationship between physical properties and temperature of materials under programmed temperature control [10]. Among the thermal analysis methods, thermogravimetry (TG), differential thermal analysis (DTA) and differential scanning calorimetry (DSC) are commonly used [11]. Thermogravimetry (TG) is to measure the relationship between the mass and temperature of the material under the temperature controlled by program. The relationship between the mass and temperature was recorded, i.e. the thermogravimetric curve (TG) [12]. Differential scanning calorimetry (DSC) is a technique to measure the power difference between the material and the reference material under the temperature controlled by program. According to the different measurement methods, this technique can be divided into power compensation differential scanning calorimetry and heat flow scanning calorimetry. The measured curve is called differential scanning calorimetry (DSC) [13].

The thermos-balance analysis method is to study the mass change law of solid and liquid fuel with time under the condition of temperature programmed, to analyze the combustion process of the samples [14]. Especially with the help of computer, a series of characteristic values of combustion process can be obtained through digital data acquisition and processing, such as ignition temperature, burnout temperature, burnout time, maximum weight loss temperature, maximum weight loss rate, combustion amount in the early and late stages of combustion, etc. [15]. And through

the combination analysis of these data, we can realize the scientific evaluation of the combustion characteristics of solid and liquid fuels.

In this manuscript, coconut shell, coal water slurry, and biomass compression molding particles were used as raw materials, and thermogravimetric analysis system was used to carry out the experiment. The reaction atmosphere was air, the flow rate was  $50 \text{ ml min}^{-1}$ , the protective gas was nitrogen ( $\text{N}_2$ ). The samples were heated from 30 to  $1000 \text{ }^\circ\text{C}$  at  $20 \text{ }^\circ\text{C min}^{-1}$  and  $40 \text{ }^\circ\text{C min}^{-1}$ . The effects of different kinds of raw materials and heating rates on the combustion characteristics of three samples were studied, and the basic combustion rules and key parameters of three samples were obtained.

## Methods

### Materials

Coconut shell (Fig. S1a) was sampled from a biomass power plant of the Hainan province, China, while biomass particles (Fig. S1c) was gathered from a biomass gasification plant of the Shandong province, China. The coconut shell and biomass particles for experiment were initially broken into small pieces, washed with distilled water, and then dried to remove residual water for one hour at  $110 \text{ }^\circ\text{C}$ . And then, the dried samples were further crushed in the pulverizer to below  $80 \text{ }\mu\text{m}$ . Coal water slurry sample (Fig. S1b) was prepared in the laboratory. Raw coal sample was milled by a coal mill with an average particle size of  $30$  to  $60 \text{ }\mu\text{m}$ . Water and additives were added according to a certain concentration ratio, and then pulverized coal was gradually added. After high-speed stirring, the coal water slurry sample was prepared. The concentration of the prepared coal water slurry was about  $65\%$ , the viscosity was  $970 \text{ mPa s}$ , and the average volume particle size was  $30.5 \text{ }\mu\text{m}$ . The physical and chemical properties of samples are summarized in Table 1.

### Experimental methods

#### Thermal analysis tests

Thermal analysis tests (Thermogravimetry, TG; Differential thermogravimetry, DTG; and Differential scanning calorimetry, DSC) were conducted on a STA 449C simultaneous thermal analyzer (NETZSCH, Germany; temperature up to  $1600 \text{ }^\circ\text{C}$ ; heating rate up to  $100 \text{ }^\circ\text{C min}^{-1}$ ; balance sensitivity of thermogravimetric analyzer is  $\pm 0.023 \text{ }\mu\text{g}$  and temperature accuracy is  $\pm 0.3 \text{ }^\circ\text{C}$ ). The samples were heated from 30 to  $1000 \text{ }^\circ\text{C}$  at  $20 \text{ }^\circ\text{C min}^{-1}$  and  $40 \text{ }^\circ\text{C min}^{-1}$ . The reaction atmosphere is air, the flow rate is  $50 \text{ ml min}^{-1}$ , the protective gas is nitrogen ( $\text{N}_2$ ), and the hanging design of upper balance is adopted to prevent the volatilization residue after sample decomposition from polluting the balance. To reduce the buoyancy effect as much as possible, the crucible and counterweight are suspended on both ends of TG bracket by filament. To avoid the thermal weight error

**Table 1** Physicochemical properties of samples

Samples	Coconut shell	Coal water slurry	Biomass
Proximate analysis (wt%)			
M <sub>ad</sub>	6.88	31.64	6.84
A <sub>ad</sub>	0.49	6.52	1.28
V <sub>ad</sub>	79.51	50.47	83.38
FC <sub>ad</sub>	13.12	11.37	8.50
Ultimate analysis (wt%)			
C <sub>ad</sub>	47.37	50.19	45.63
H <sub>ad</sub>	4.91	3.23	5.67
N <sub>ad</sub>	4.53	0.64	4.75
S <sub>ad</sub>	0.02	0.90	0.02
O <sub>ad</sub>	35.81	6.90	35.83
Low calorific value (MJ kg <sup>-1</sup> )	17.92	19.73	16.94

(1) ad: air dried basis,  $M_{ad} + A_{ad} + V_{ad} + FC_{ad} = 100$ , (2) The  $O_{ad}$  was computed by mass difference:  $O_{ad} = 100 - N_{ad} - C_{ad} - H_{ad} - S_{ad}$

caused by the change of the center of gravity of the sample, the crucible is always placed in the center of the furnace chamber. In the experiment, the atmosphere was blown from top to bottom. Due to the design of the upper balance system, the sample was fully contacted with the reaction atmosphere, and the measurement error was reduced as much as possible to ensure the experimental accuracy.

### Combustion thermogravimetric tests

The carrier gas flow was set at 60 ml min<sup>-1</sup> to simulate air atmosphere (N<sub>2</sub>:O<sub>2</sub> = 4:1). The samples were taken as 20 ± 0.2 mg and non-isothermal method was used. Starting from room temperature, the final reaction temperature was 1000 °C, and the heating rate was 20 °C min<sup>-1</sup> and 40 °C min<sup>-1</sup>. To eliminate the system error and buoyancy effect, a blank test was conducted before each test, and the test results were obtained after deducting the baseline. To reduce the measurement error, each test is repeated several times to ensure the accuracy, and the test results have high repeatability.

### Other tests

The stiffness of the samples was measured by stiffness meter (HAAKE VT550) produced by thermo company in Germany, and the particle size of coal water slurry samples was measured by Malvern laser particle size analyzer (Mastersizer 2000).

## Data processing method of combustion characteristics

For the combustion test results, the following analysis parameters are introduced for easy Description:

### Ignition temperature $T_i$

The ignition temperature, corresponding to the temperature at which the sample begins to burn, is an important parameter to measure the ignition characteristics of the sample [16]. The lower the ignition temperature is, the easier it is to ignite. As shown in Fig. S2, the ignition point of samples is determined by TG–DTG joint definition. A vertical line is drawn through the maximum weight loss point of DTG curve and intersects with TG curve. Then the tangent line of TG curve is made through this intersection point, which intersects with the parallel line of mass loss at the beginning of TG curve, which is the ignition temperature  $T_i$ .

### Burnout temperature $T_h$

The burnout temperature corresponds to the point where there is no mass change in TG and DTG curves. When the mass loss of combustibles reaches 98% of the total mass loss, the corresponding temperature is the burnout temperature  $T_h$  [17].

### Combustion characteristic

To comprehensively analyze the combustion characteristics of the samples, the comprehensive combustion characteristic index  $S_N$  was used to analyze the test results [18].  $S_N$  is calculated according to Eq. (1).

$$S_N = \frac{(dm/dt)_{\max} (dm/dt)_{\text{mean}}}{T_i^2 T_h} \quad (1)$$

Here,  $(dm/dt)_{\max}$  and  $(dm/dt)_{\text{mean}}$  are the maximum and mean combustion rates.

### Thermo-kinetics analysis by Coats–Redfern method

Biomass and coal combustion is a typical gas–solid reaction. Gas solid reaction can be divided into gas–solid reaction with solid products and gas–solid reaction without solid products. According to the structural characteristics of solids, solid reactants can be divided into dense solids and porous solids. Biomass and coal particles are porous solids. Ash is generated during combustion, which is a gas–solid reaction with solid products. The combustion process is irreversible and the equilibrium constant of gas–solid reaction tends to infinity. External diffusion resistance and chemical reaction resistance derived by the comprehensive rate equations of internal diffusion resistance, it is assumed that the mass transfer rate of the boundary layer is equal to the internal diffusion rate of the solid product layer and the consumption rate of the reaction interface [19]. The results are as follows,

$$\frac{b}{\rho} \frac{k}{R_0} C_0 t = \frac{k\alpha}{h_m f_s} + \frac{kR_0}{2D_e f_s} \times \left[ 1 + 2(1 - \alpha) - 3(1 - \alpha)^{\frac{2}{3}} \right] + 1 - (1 - \alpha)^{\frac{1}{3}} \quad (2)$$

$$\frac{b}{\rho} \frac{k}{R_0} C_0 t = \frac{k\alpha}{h_m f_s} + \frac{kR_0}{2D_e f_s} \times [\alpha + (1 - \alpha) \ln(1 - \alpha)] + 1 - (1 - \alpha)^{\frac{1}{3}} \quad (3)$$

$$\frac{b}{\rho} \frac{k}{R_0} C_0 t = \frac{k\alpha}{h_m f_s} + \frac{kR_0}{2D_e f_s} \alpha^2 + \alpha \quad (4)$$

Here,  $b$  is the stoichiometric coefficient of gas–solid reaction;  $\rho$  is the particle density, mol m<sup>-3</sup>;  $k$  is the reaction rate constant;  $R_0$  is the characteristic size of particles, m;  $C_0$  is the concentration of gas phase reactant in the main body of gas phase, mol m<sup>-3</sup>;  $C_1$  is the concentration of the gas phase product in the main body of the gas phase, mol m<sup>-3</sup>;  $t$  is time, s;  $D_e$  is the effective diffusion coefficient, m<sup>2</sup> s<sup>-1</sup>;  $f_s$  is the particle shape factor,  $f_s = \frac{R_0 A}{V}$ ;  $A$  is the surface area of particles, m<sup>2</sup>;  $V$  is the particle volume, m<sup>3</sup>;  $\alpha$  is the conversion rate,  $\alpha = \frac{m_T - m_0}{m_\infty - m_0}$ ;  $m_0, m_T, m_\infty$  is the initial mass of the sample, the mass at temperature  $T$  and the residual mass after the reaction, mg;  $h_m$  is the mass transfer coefficient, m s<sup>-1</sup>.

For combustion, the three terms on the right of Eqs. 2, 3, and 4 represent the external diffusion resistance of oxygen and carbon combustion products between the gas–phase main body and the reaction boundary layer, the internal diffusion resistance of oxygen and carbon combustion products in the reaction interface layer and the combustion chemical reaction resistance in turn. The thermogravimetric analysis experiment in this study can be regarded as infinite if it is carried out under good external mass transfer conditions. Therefore, the external diffusion resistance can be ignored. When the functions  $\alpha$  of internal diffusion resistance and chemical reaction resistance on the right of Eqs. 2, 3, and 4 are expressed by  $H(\alpha)$  and  $N(\alpha)$ , then Eqs. 2, 3, and 4 can be expressed as:

$$\frac{bC_0 k}{\rho R_0} t = \frac{kR_0}{2D_e f_s} N(\alpha) + H(\alpha) \quad (5)$$

The derivation of Eq. 5 is as follows,

$$e_1 \frac{dt}{d\alpha} = H(\alpha)t + e_2 N(\alpha)t \quad (6)$$

Here  $e_1 = (bC_0 k)/(\rho R_0)$ ,  $e_2 = (R_0 k)/(2D_e f_s)$ ;  $T$  is the absolute temperature, K.

When the internal diffusion resistance is small,  $D_e$  is very large and  $e_2$  tends to zero. The reaction is controlled by chemical reaction. The second term on the right side of Eq. 6 can be ignored. The kinetic integral equation can be simplified as follows:

$$\frac{d\alpha}{dt} = \frac{e_1}{H(\alpha)t} \quad (7)$$

When the internal diffusion resistance is large, that is,  $D_e$  very small,  $e_2$  obviously greater than 1, the reaction is controlled by internal diffusion, the first term on the right of Eq. 6 can be ignored, and the kinetic integral equation can be simplified as follows:

$$\frac{d\alpha}{dt} = \frac{e_1}{e_2 N(\alpha)'} \quad (8)$$

In Eqs. 7 and 8, when the reaction is controlled by chemical reaction and internal diffusion, the control reaction mechanism functions  $f(\alpha)$  is  $1/H(\alpha)'$  and  $1/N(\alpha)'$ . In the thermogravimetric experiment, the combustion process is a non-isothermal heterogeneous reaction process, and the reaction rate equation is as follows,

$$\frac{d\alpha}{dT} = \left(\frac{1}{\beta}\right) k(T) f(\alpha) \quad (9)$$

Here  $k(T)$  is the temperature relation of reaction rate constant;  $\beta$  is the heating rate,  $K \text{ min}^{-1}$ .

By introducing the Arrhenius rate constant–temperature relation  $k = A \exp[-E/(RT)]$  [20], Eq. 9 can be changed into as follow,

$$\frac{d\alpha}{dT} = \frac{A}{\beta} f(\alpha) \exp\left(-\frac{E}{RT}\right) \quad (10)$$

Here  $A$  is the pre-exponential factor,  $\text{min}^{-1}$ ;  $E$  is the activation energy,  $\text{J mol}^{-1}$ ;  $R$  is the gas constant,  $\text{J K}^{-1} \text{ mol}^{-1}$ ;  $T$  is the absolute temperature,  $\text{K}$ .

The combustion mass reduction process is described by Eq. 11.

$$f(\alpha) = (1-\alpha)^n \quad (11)$$

The conversion rate  $\alpha$  is calculated according to Eq. 12.

$$\alpha = \frac{m_0 - m_T}{m_0 - m_\infty} \quad (12)$$

The Coats–Redfern method is used for dynamic treatment, and Eq. 10 can be integrated [21],

$$\ln \left[ \frac{G(\alpha)}{T^2} \right] = \ln \frac{AR}{\beta E} - \frac{E}{RT} \quad (13)$$

Therefore, when the reaction is controlled by chemical reaction and internal diffusion,  $G(\alpha)$  is  $H(\alpha)$  and  $N(\alpha)$ , respectively. A straight line can be obtained by plotting  $\ln[G(\alpha)/T^2]$  to  $1/T$ , and the dynamic parameters  $E$  and  $A$  can be obtained by the slope and intercept of the straight line.

## Results and discussion

### Combustion thermogravimetric analysis

#### Effect of different heating rates on combustion thermogravimetry

TG, DTG, and DSC curves of coconut shell, coal water slurry, and biomass combustion at different heating rates ( $20\text{ }^{\circ}\text{C min}^{-1}$  and  $40\text{ }^{\circ}\text{C min}^{-1}$ ) are shown in Figs. 1, 2, and 3.

In Figs. 1 and 3, the TG, DTG, and DSC curves of coconut shell and biomass at different heating rates ( $20\text{ }^{\circ}\text{C min}^{-1}$ ,  $40\text{ }^{\circ}\text{C min}^{-1}$ ) have similar trends. From the beginning of combustion to  $200\text{ }^{\circ}\text{C}$ , there is a small weight loss step in TG curve, and the weight loss is about 3% to 5%. The first stage corresponds to the large loss of free water and the release of a small amount of small molecule volatiles. TG curve decreased slightly and mass loss was slow. The second stage of combustion is  $200\text{ }^{\circ}\text{C}$  to  $500\text{ }^{\circ}\text{C}$ . There is an obvious mass loss process in the corresponding TG

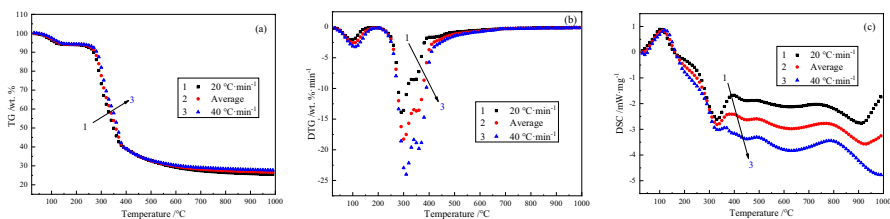


**Fig. 1** TG, DTG, and DSC curves of coconut shell at different heating rates. **a** TG, **b** DTG, **c** DSC

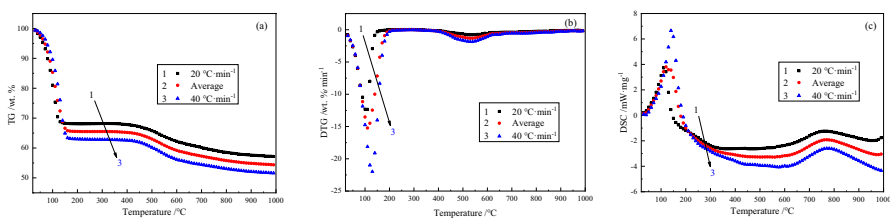


**Fig. 2** TG, DTG, and DSC curves of coal water slurry at different heating rates. **a** TG, **b** DTG, **c** DSC

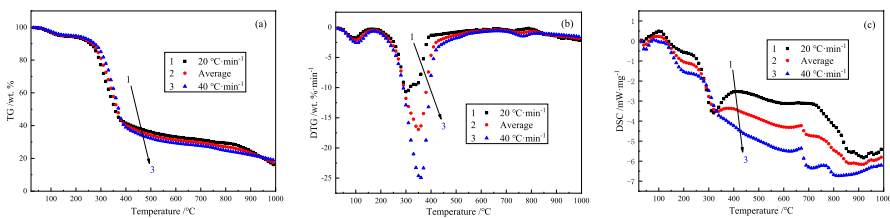


**Fig. 3** TG, DTG, and DSC curves of biomass at different heating rates. **a** TG, **b** DTG, **c** DSC



curve, and the weight loss is about 40% to 60%. In the second stage, a large amount of volatile matter and fixed carbon combustion of a small amount of fixed carbon were observed, which showed that the TG curve decreased rapidly and the mass loss was obvious. 500 °C to 900 °C is the third stage of combustion, and the corresponding TG curve has a large weight loss step, and the weight loss is about 10% to 40%. The third stage corresponds to the continuous fixed carbon combustion of a large amount of fixed carbon and a small amount of residual volatile matter, which shows that the curve continues to decline significantly and the mass loss further, but the decline is not as steep as that in the second stage.

There are three mass loss peaks in the DTG curve at combustion stages. The first peak is relatively gentle because the water content of the sample is low and the mass loss is not obvious. The second peak is high and sharp, mainly due to the high volatile content in the sample, which is more than 75% (Coconut shell 79.51%, Biomass 83.38%), and the volatile combustion rate is faster. The third peak is lower and wider than the second peak, which is due to the relatively small fixed carbon content (Coconut shell reaches 13.12%, Biomass reaches 8.50%), and combustion is relatively not concentrated.

In Fig. 2, the TG, DTG, and DSC curves of coal water slurry can be divided into three main stages. From the beginning of combustion to 200 °C, there is a small weight loss step in TG curve, and the weight loss is about 25% to 30%. In the first stage, the TG curve decreased rapidly, corresponding to the large loss of external water and internal free water and the release of a small amount of small molecule volatiles. The second stage of combustion is 200 °C to 650 °C. There is an obvious mass loss process in the corresponding TG curve, and the weight loss is about 10% to 20%. In the second stage, the TG curve decreased slightly and the mass loss was obvious. 650 °C to 850 °C is the third stage of combustion, and the corresponding TG curve has a small weight loss step, and the weight loss is about 5% to 10%. The third stage corresponds to the decomposition and combustion of residual carbon and low active combustible components, and the TG curve decreases slowly until smooth.

There are three mass loss peaks in DTG curve at three combustion stages. The first peak is relatively gentle because the water content of coal water slurry is high and the mass loss is obvious. The second peak is high and has a long span, which is mainly due to the high volatile content and low fixed carbon content (volatile content 50.47%, fixed carbon content 11.37%), so the combustion is relatively stable and lasting. The third peak has a small span and low peak value, which is mainly due to the low content of residual carbon and low active combustible components and slow reaction.

In Figs. 1, 2, 3, with the increase of heating rate, the peak value of weight loss rate of sample combustion increases, and the temperature corresponding to the peak value increases. All reaction stages in the combustion process move to the high temperature side, and the mass loss in the whole combustion process is less concentrated. The main reason is that with the increase of heating rate, the temperature difference between the sample and the furnace increases in a short time, which leads to the increase of particle temperature gradient in the sample, which aggravates the heat transfer lag. According to the TG curve, the final weight loss rate of the same

sample at different heating rates has little change, which indicates that the different heating rates have little effect on the total weight loss. The DTG curve shows that the weight loss rate of the same sample is significantly different under different heating rates, which indicates that different heating rates have great influence on the weight loss rate. With the increase of heating rate, the weight loss rate increases obviously.

### Effect of the same heating rate on combustion thermogravimetry

The TG, DTG, and DSC curves of coconut shell, coal water slurry and biomass combustion at the same heating rate ( $40\text{ }^{\circ}\text{C min}^{-1}$ ) are shown in Fig. 4.

There is a weight loss step in the TG curve of the first stage, which corresponds to the large loss of free water in the sample and the release of a small amount of small molecule volatiles. The TG curve of coconut shell and biological production decreased slightly, and the mass loss was slow, while the external water content of coal water slurry was more, which showed that the TG curve obviously decreased and the mass loss was large. Then, the TG curve of the second stage corresponds to the combustion of a large amount of volatile matter and fixed carbon combustion of a small amount of fixed carbon. The TG curve of coconut shell and biomass decreases rapidly and the mass loss is obvious, while the TG curve of coal water slurry decreases slightly and the mass loss is slow due to less volatile matter. Next, the TG curve of the third stage corresponds to the continuous fixed carbon combustion of fixed carbon and a small amount of residual volatile matter. The curves of coconut shell, coal water slurry, and biomass continue to decline significantly, and the quality of coconut shell, coal water slurry, and biomass is further reduced, but the decline range is not as steep as that in the second stage. And then, the TG curves of coconut shell, coal water slurry and biomass decrease slowly until smooth.

### Combustion characteristics analysis

The combustion characteristic parameters of coconut shell, coal water slurry, and biomass combustion at different heating rates ( $20\text{ }^{\circ}\text{C min}^{-1}$ ,  $40\text{ }^{\circ}\text{C min}^{-1}$ ) are shown in Table 2.

In Table 2, with the increase of heating rate from  $20$  to  $40\text{ }^{\circ}\text{C min}^{-1}$ , the ignition temperature of coconut shell increases from  $273.16$  to  $279.19\text{ }^{\circ}\text{C}$ , the burnout

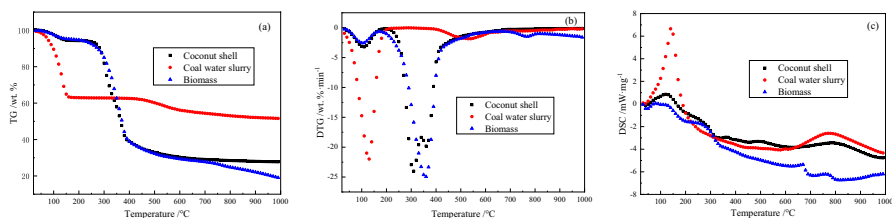


**Fig. 4** TG, DTG, and DSC curves of coconut shell, coal water slurry and biomass at heating rate of  $40\text{ }^{\circ}\text{C min}^{-1}$ . **a** TG, **b** DTG, **c** DSC

**Table 2** Combustion characteristic parameters of coconut shell, coal water slurry, and biomass

Samples	Heating rate $\beta$ ( $^{\circ}\text{C min}^{-1}$ )	Ignition tempera- ture ( $T_i/^{\circ}\text{C}$ )	Burnout tempera- ture ( $T_b/^{\circ}\text{C}$ )	Maximum burning rate ( $\text{dm}/\text{dt}$ ) <sub>max</sub> ( $\% \text{ min}^{-1}$ )	Average burning rate (dm/ dt) <sub>mean</sub> ( $\% \text{ min}^{-1}$ )	Comprehensive combustion characteristic index $S_N/10^{-7}$
Coconut shell	20	273.16	740.21	14.2186	1.5371	3.9570
	40	279.19	690.78	24.0591	2.9804	13.3172
Coal water slurry	20	112.21	851.88	12.7566	0.9159	10.8933
	40	135.23	850.82	22.0218	1.9951	28.2376
Biomass	20	249.71	982.43	10.7956	1.7481	3.0804
	40	257.46	955.47	24.9997	3.3508	13.2266

temperature decreases from 740.21 to 690.78 °C, the maximum combustion rate increases by 169%, and the average combustion rate increases by 1.94%. The ignition temperature of coal water slurry increases from 112.21 to 135.23 °C, the burnout temperature increases from 851.88 to 850.82 °C, the maximum combustion rate increases by 1.73%, and the average combustion rate increases by 218%. The ignition temperature of biomass increased from 249.71 to 257.46 °C, the burnout temperature decreased from 982.43 to 955.47 °C, the maximum combustion rate increased by 232%, and the average combustion rate increased by 192%. With the increase of heating rate, the overall combustion trend of coconut shell, coal water slurry, and biomass remains the same, but the specific combustion range has a certain deviation. With the increase of heating rate, the ignition temperature of the sample shifts about 10 °C to the high temperature region, and the burnout temperature shifts 1 to 50 °C to the low temperature region, and the higher the heating rate, the more obvious the shift.

As shown in Table 2, at the same heating rate, the  $S_N$  of coal water slurry is the highest, and the combustion characteristics become worse obviously. In addition, the  $S_N$  of coconut shell, coal water slurry and biomass increased by 337%, 259% and 429% when the heating rate increased from 20 to 40 °C min<sup>-1</sup>, which indicated that increasing the heating rate could improve the combustion characteristics of the samples.

## Thermokinetics analysis

To determine the combustion reaction mechanism of the three samples, the combustion reaction section of the sample data is selected to plot  $\ln[G(\alpha)/T^2]$  and  $1/T$ . The results are shown in Fig. 5, the combustion process of coconut shell is similar to that of biomass but very different from that of coal water slurry. During the combustion process, the  $\ln[G(\alpha)/T^2]$  value of the coconut shell combustion reaction significantly exceeds that of the biomass combustion reaction at all reaction stages as the temperature inverse  $1/T$  rises. This difference is mainly attributed to the higher content of elemental carbon in coconut shell than in biomass, as shown in Table 1. In the whole reaction process, there are obvious differences between  $\ln[G(\alpha)/T^2]$  and  $1/T$  in high temperature and low temperature, showing two different linear relationships. Therefore, it is necessary to analyze the combustion process of the three samples in different stages.

When the heating rates of the three samples are 20 °C min<sup>-1</sup> and 40 °C min<sup>-1</sup>, and the reaction order is 1 and 2, the reaction mechanism functions of the three samples are calculated and compared in Tables S1, S2, and S3. According to the correlation degree of the final fitting line, the most probable mechanism function of the combustion power of the three samples was determined, and then the most probable reaction mechanism and kinetic parameters of the samples were obtained.

Table S1 and S3 show that the reaction mechanism of coconut shell and biomass in low temperature section is sheet inner diffusion mechanism. In the low temperature range, the intrinsic chemical reaction rate of the first reacting combustible material is fast enough, and the reaction rate is controlled as the diffusion

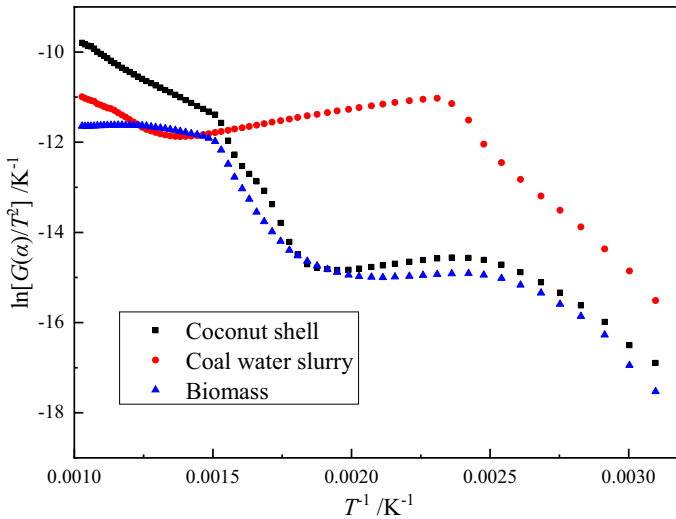


**Fig. 5** Relationship between  $\ln[G(\alpha)/T^2]$  and  $1/T$  during the combustion of different samples

rate of oxygen. When oxygen diffuses to the reaction interface, it is consumed immediately. Therefore, when the temperature of the material exceeds the reaction temperature required by the combustibles in the low temperature section, the reaction rate increases sharply, which is consistent with the DTG curves in Figs. 1 and 3. With the consumption of combustibles, the reaction interface moves inward gradually, so the reaction is controlled by one-dimensional diffusion from the surface to the inside. The combustion reaction mechanism of high temperature section is the control mechanism of spherical interface chemical reaction. Because in the low temperature section, after the flammable substances in coconut shell are burned out, the combustion substances in the high temperature section are more difficult to react, and the intrinsic chemical reaction rate of this part of carbon is smaller, so the reaction rate is controlled as the intrinsic chemical reaction stage of coconut shell. It can be seen from Tables S1, S2, and S3 that the comprehensive combustion performance of coconut shell is higher than that of biomass, and the reaction activation energy is higher than that of biomass at high temperature.

In Table S2, the combustion process of coal water slurry is quite different from that of coconut shell and biomass. In terms of water evaporation, there is a large amount of free water in coal water slurry, so the temperature of water evaporation is low. In the low temperature stage, the fuel components have not reacted yet, which is mainly due to the heat consumption of water evaporation in coal water slurry. When the temperature of the material exceeds the temperature required for water evaporation, the combustion reaction of coal water slurry begins. The combustion reaction mechanism in the high temperature section is the spherical interface chemical reaction control mechanism. This is consistent with the DTG curve in Fig. 2. With the consumption of combustibles, the reaction interface moves inward gradually.

According to the comparative analysis of Tables S1, S2, and S3, the fitting correlation coefficient  $R^2$  of three samples and the average fitting effect of reaction level  $n=2$  are better than that of  $n=1$ . The activation energy of coconut shell at low temperature was 33.33 to 79.08 kJ mol<sup>-1</sup>, which was significantly higher than that at high temperature (19.99 to 25.64 kJ mol<sup>-1</sup>); The activation energy of coal water slurry at low temperature range is 19.68 to 47.94 kJ mol<sup>-1</sup>, which is significantly higher than that at high temperature range 18.99 to 29.22 kJ mol<sup>-1</sup>; The activation energy of biomass in low temperature range is 30.22 to 78.21 kJ mol<sup>-1</sup>, which is significantly higher than that in high temperature range of 1.49 to 12.12 kJ mol<sup>-1</sup>; When the value of  $n$  is set to 2, the resulting fitting curve exhibits a notably strong linear relationship. Furthermore, the correlation coefficients, denoted as  $R^2$ , are consistently above 0.99, a figure that is indicative of a highly significant correlation. This finding suggests that the combustion kinetics of the three samples studied can be accurately represented and predicted by the set reaction order of 2. In essence, the strong linearity and high correlation coefficients provide compelling evidence that the chosen order of reaction aptly captures the characteristics of the combustion process in these samples.

Due to the existence of water in coal water slurry, its calorific value is lower than that of coal used for coal water slurry, so the combustion temperature of coal water slurry is low, which is suitable for low temperature combustion. The actual combustion shows that the furnace combustion temperature is lower than that of oil and coal (about 100 °C), which can greatly reduce the emission of SO<sub>2</sub>. Due to its combustion mode, it is also conducive to the control of NO<sub>2</sub> generation. The existence of water in coal water slurry can help coal slurry spray evenly and disperse, which is conducive to the rapid and complete combustion of carbon. At the same time, the existence of water vapor in gas can increase the radiation intensity of flame and improve the heat transfer effect.

## Conclusions

Coconut shell, coal water slurry, and biomass compression molding particles were used as raw materials, and thermogravimetric analysis system was used to carry out the experiment. The effects of different kinds of raw materials and heating rates on the combustion characteristics of three samples were studied, and the basic combustion rules and key parameters were obtained. The DTG curves of coconut shell, coal water slurry curve, and biomass combustion show three mass loss peaks. The heating rate has little effect on the burnout of coconut shell, coal water slurry, and biomass. At low combustion rates, sufficient combustion reaction time should be ensured. At the same heating rate, the  $S_N$  of coal water slurry is the highest, the  $S_N$  of coconut shell, coal water slurry and biomass increased by 337%, 259%, and 429% when the heating rate increased from 20 to 40 °C min<sup>-1</sup>, which indicated that increasing the heating rate could improve the combustion characteristics of the samples. All three samples showed higher activation energy in the low temperature combustion zone. As the heating rate increases, the activation energy of the sample decreases slightly, but the overall trend remains unchanged. When  $n=2$ , the fitting

curve has a good linear relationship, and the correlation coefficient  $R^2$  is all above 0.99.

**Supplementary Information** The online version contains supplementary material available at <https://doi.org/10.1007/s11144-024-02633-x>.

**Acknowledgements** This work was supported by “Research on new pyrolysis gasification technology for biomass YFHT-1904”.

**Data availability** All data have been properly stored in the study and are available to other researchers upon reasonable request. To ensure the accuracy and completeness of the data, we are willing to share the data with interested researchers and assist them in understanding and using the data. To obtain data, please contact us via email and we will respond as soon as possible and provide the required data support. We hereby pledge to respond positively and do our best to fulfill reasonable data sharing requests.

## Declarations

**Conflict of interest** This article content has no conflict of interest.

## References

1. Hu S, Jiang F, Zhao B, Chen Y, Liu K (2021) *Energy Fuel* 35(3):2006–2015
2. Lin L, Ma C, Hu S, He H, Yu H, Wang Q, Cao X, You X (2021) *Int J Min Sci Technol* 31(3):515–521
3. Atesok G, Ozer M, Boylu F, Dincer H (2005) *Int J Miner Process* 77(4):199–207
4. Kuznetsov G, Nyashina G, Strizhak P, Valiullin T (2021) *J Energy Inst* 97:213–224
5. Wang Z, Huang W, Wang H, Gao J, Zhang R, Xu G, Wang Z (2024) *J Clean Prod* 434:140365
6. Yuan Y, Zuo H, Wang J, Gao Y, Xue Q, Wang J (2022) *Fuel* 324:124727
7. Balmuk G, Cay H, Duman G, Kantarli I, Yanik J (2023) *Energy* 278:127803
8. Zhou Y, Xu G, Li H, Chen Y, Xu X, Li M (2023) *Environ Res* 238:117184
9. Huang X, Yin H, Zhang H, Mei N, Mu L (2022) *Energy* 259:125062
10. Fuse H, Tomita F, Fujisaki T, Yasue K, Miyakawa S, Koori N, Abe S (2024) *Radiat Phys Chem* 217:111458
11. Tang Z, Chen Y, Liu J, Cheng W, Wang X, Hu Q, Yang Y, Yang H, Chen H (2024) *J Anal Appl Pyrol* 177:106333
12. Zhao Y, Hu H, Jin L, He X, Wu B (2011) *Fuel Process Technol* 92:780–786
13. Benke M, Tranta F, Barkóczy P, Mertinger V, Daróczy L (2008) *Mater Sci Eng A* 481–482:522–525
14. Chanin H, Pramono H, Aziz M (2022) *Sustain Energy Technol* 51:101968
15. Hsuan C, Hou S (2022) *Fuel* 362:130821
16. Zhang Y, Zhang Y, Li Y, Shi X, Che B (2022) *Energy* 240:122493
17. Zeng X, Zheng S, Zhou H, Fang Q, Lou C (2016) *Appl Therm Eng* 103:1156–1163
18. Wei P, Ning X, Zhou Y, Liu J, Yu J (2011) *Adv Mater Res* 391–392:1440–1444
19. Akaln K (2012) *J Therm Anal Calorim* 109(1):227–235
20. Criado J, Ortega A (1985) *Int J Chem Kinet* 17(12):1365–1373
21. Zhu F, Feng Q, Xu Y, Liu R, Li K (2015) *J Therm Anal Calorim* 119(1):651–657

**Publisher's Note** Springer Nature remains neutral with regard to jurisdictional claims in published maps and institutional affiliations.

Springer Nature or its licensor (e.g. a society or other partner) holds exclusive rights to this article under a publishing agreement with the author(s) or other rightsholder(s); author self-archiving of the accepted manuscript version of this article is solely governed by the terms of such publishing agreement and applicable law.